41st Plasmadynamics and Lasers Conference
28 June - 1 July 2010, Chicago, Illinois

AIAA 2010-4630

Experimental Study on the Body Force Field of Dielectric Barrier Discharge Actuators

Marios Kotsonis*, Sina Ghaemi†, Rogier Giepman‡ and Leo Veldhuis§
Delft University of Technology, Delft, 2629HS, The Netherlands

An experimental investigation on thrust and body force of Dielectric Barrier Discharge (DBD) /plasma actuators aimed at low power flow control applications is presented. A parametric study on thrust is conducted for a wide range of geometrical configurations as well as several electrical operational conditions. Direct measurements of the induced thrust are taken using a highly sensitive load cell. Simultaneous readings of current and voltage are also performed, providing the power consumption. Furthermore a novel technique for determination of the spatial distribution of the body-force is proposed, developed and tested. The technique involves the use of a high-speed PIV system to resolve all terms of the Navier-Stokes equation representation of the flow field including body force. Results reveal the existence of an explicit relation between voltage, thrust and consumed power. Furthermore the influence of the geometrical configuration of the actuator on the thrust is shown. The body force obtained with the proposed technique agrees well with the thrust measurements.

I. Introduction

Plasma actuators have been studied extensively in recent years, as flow control devises. Their low power consumption, lack of moving parts and robustness render them ideal for flow manipulation. There are several implementations of the actuators the most popular being the Dielectric Barrier Discharge (DBD) kind (Fig.1). These are based on the ionization of air via an AC High Voltage (HV) signal. Two electrodes are usually employed one being grounded, the other carrying the HV signal. The electrodes are separated by a dielectric layer which prohibits arc forming and allows for the ionized gas to accumulate on the surface. The exact mechanisms of the interaction between the weakly ionized gas and neutral air are still debated. It is, nevertheless, commonly accepted that some sort of collisional processes between the heavy plasma species (mostly ions) and neutral air is responsible for the momentum transfer. In a macroscopic scale, which is usually the scale of the flow to be controlled, the model of an exerted body force on the fluid seems to describe the effect reasonably.

Plasma actuators have been used in several studies aiming at separation control,[1] turbulent drag reduction,[2] boundary layer control[3–5] and transition delay.[6] Excellent reviews on plasma actuators for aerodynamic flow control have been published recently.[7,8]

The capabilities of the actuators suggest the feasibility of their implementation in several flow control scenarios. It is therefore desirable to have an efficient and accurate model of the effect of the actuator on a given flow. A large amount of simulation studies has been conducted in order to simulate and capture the underlying physics of the ionization process.[9,10] These vary in model complexity, from simple phenomenological models to first principles fluid models.[11] Extended simulations for multi-species fluids have also been investigated.[12] In the majority of these modeling approaches the final goal is to determine the exerted body force on the fluid. A number of studies on flow solvers implementing plasma actuators have used this approach successfully to couple the effect of the actuator with the flow dynamics.[13–15]

*PhD researcher, Faculty of Aerospace Engineering, Kluyverweg 1.
†PhD researcher, Faculty of Aerospace Engineering, Kluyverweg 1.
‡MSc Student, Faculty of Aerospace Engineering, Kluyverweg 1.
§Assistant Professor, Faculty of Aerospace Engineering, Kluyverweg 1, AIAA Member.

Apart from the modeling efforts the experimental investigation on the actuator's operation has also received substantial attention. Several studies focus on the investigation of the induced flow field and the produced thrust from the actuators.[16,17] These two quantities can lead to an estimation of the space domain integrated magnitude of the exerted body force. These techniques and others have been used successfully by researchers for investigations and parametric studies on plasma actuators. They are robust and fast although they present some drawbacks which render the results difficult to be used as an input in flow solvers, an area that so far has been served only by numerical plasma modeling studies. An inherent disadvantage for these techniques is that part of the measured thrust is not to be credited to the actuator but to the shear forces that develop between the induced flow and the flat surface. The main disadvantage of these techniques, though, is their inability to give any information on the spatial distribution of the force field, information that is vital in cases of discrete, unsteady and localized actuation proposed by the majority of flow control concepts. To the authors's knowledge there has yet been an investigation on the determination of both the magnitude and the spatial distribution of the body force vector field.

In this paper an investigation on the thrust and body force of the plasma is performed. A novel technique is proposed, developed and tested to accurately and efficiently measure the body force magnitude, spatial distribution and orientation in the vicinity of the actuator. After an overview of the methodology a description of the experimental setup is given which is followed by a discussion on the results. Finally some conclusions and future work are presented.

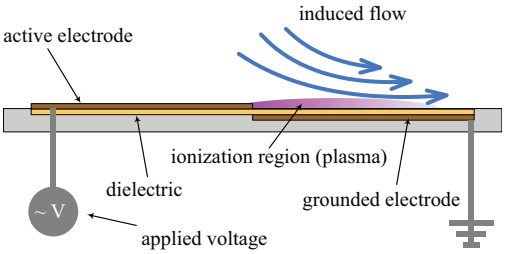

Figure 1. Geometrical configuration and operation of the plasma actuator

II. Methodology

The determination of the induced body force can be done experimentally in several ways. Nevertheless due to the nature of the momentum transfer mechanisms only indirect methods based on the induced flow field or reaction forces can be feasibly employed in the time span such an experiment allows. In this study two techniques are applied to determine thrust and one technique to determine body-force. More specifically the techniques employed are: direct thrust measurements using a highly sensitive load cell, thrust calculation via momentum balance of the induced flow field and body-force estimation using high speed PIV data of the accelerating flow field.

A. Direct thrust measurement

Direct thrust measurement is the most straightforward from the tested techniques. It simply involves attaching the actuator on a load cell and and measuring the force exerted by the induced flow on the actuator. By means of Newton's third law this force is equal and opposite to the total force the actuator exerts on the flow. Although this is a very simple and robust technique, some further clarifications must be made on what exactly is being measured. It has been reported repeatedly and also verified in this work that the induced flow field from the continuous operation of the actuator resembles a typical laminar wall jet. As such a certain shear force develops on the wall surface of the actuator which is also measured by the load cell. This has to be taken under account as it is not directly related to the body-force the actuator exerts on the flow. An other issue with this technique, and generally all techniques that deal with integrated values such as thrust, is that an estimation can be given on the magnitude of the body-force but not on its spatial distribution.

B. Thrust calculation from velocity measurements

The second technique investigated is based on existing measurements of the induced velocity profile across the formed jet. A control volume approach is then taken where the momentum flux is calculated and equilibrium with the exerted force is assumed (Fig.2). For all subsequent figures and references to distance, the displayed coordinate system is used. The origin lies at the downstream end of the exposed electrode and on the flat surface. The calculated thrust is then the net thrust from the actuator with the effects of skin friction at the wall also taken into account. This technique also suffers from lack of any information on the spatial distribution of the body force. More specifically applying the momentum balance equation on the control volume gives:

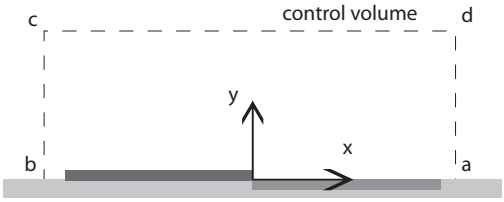

Figure 2. The control volume for the momentum balance equations

$$\vec{F} = \oint_{abcd} (\rho \vec{U} \cdot dS)\vec{U} + \oint_{abcd} pdS \tag{1}$$

where $\vec{F}$ is the body force exerted on the fluid, $\vec{U}$ is the velocity field, ρ is the density and p is static pressure. Eq.1 is developed for the boundaries taking account the no-slip condition at the wall. Note that the boundaries where the unit vector perpenticular to the surface (dS) is negative take a minus sine:

- x -direction

$$F_x = \rho \int_{da} {u_x}^2 dy + \rho \int_{cd} u_x u_y dx - \rho \int_{bc} {u_x}^2 dy + \int_{da} p dy - \int_{bc} p dy \tag{2}$$

- y -direction

$$F_y = \rho \int_{da} u_x u_y dy + \rho \int_{cd} {u_y}^2 dx - \rho \int_{bc} u_x u_y dy + \int_{cd} p dx - \int_{ba} p dx \tag{3}$$

Due to the fact that pressure is not readily available from velocity data a further assumption needs to be made. This states that if the control volume boundaries are far enough from the bulk of the plasma body force (near the inner electrode edge) pressure can be considered uniform and equal. This is justified since the induced flow field is not pressure driven but rather initiated by the actuator. It should also be noted here that for the x-direction the calculated force (F_x) contains not only the contribution of the plasma actuator (F_x^p) but also the shear force between the flow and the surface (F_x^s). These assumptions reduce Eq.2 and Eq.3 to

- x -direction

$$F_x^p + F_x^s = \rho \int_{da} {u_x}^2 dy + \rho \int_{cd} u_x u_y dx - \rho \int_{bc} {u_x}^2 dy \tag{4}$$

- y -direction

$$F_y = \rho \int_{da} u_x u_y dy + \rho \int_{cd} {u_y}^2 dx - \rho \int_{bc} u_x u_y dy \tag{5}$$

C. Body-force calculation from PIV data

The third technique investigated is a novel approach in determining the full body-force field both in magnitude and spatial distribution. It involves the measurement of the induced flow-field using a two component high-speed PIV system. The evolution of the flow field is recorded starting prior to the actuation where the flow is quiescent and continuing until the flow has reached steady state. By resolving the flow field both in space and time, an analysis based on the full Navier-Stokes equations can provide the body-force. More

specifically: Consider the attained 2D flowfield $\vec{U}(x, y, t)$ from the PIV measurements. The 2D incompressible NS equations in the presence of body-forces read:

$$\frac{\partial \vec{U}}{\partial t} + \vec{U} \cdot \nabla \vec{U} - \nu \, \nabla^2 \vec{U} = -\nabla p + \frac{\vec{F}}{\rho} \tag{6}$$

A first approach in deriving the body force is to apply Eq.6 only for the first moments after the actuation. During this stage the flow accelerates only around the region of the applied body force where the rest of the field is still relatively quiescent. This implies that the convective, viscous and pressure gradient terms are relatively small and can be neglected. This reduces Eq.6 to:

$$\frac{\partial \vec{U}}{\partial t} = \frac{\vec{F}}{\rho} \tag{7}$$

which is basically Newton's second law. This method will be referenced as the 'reduced method' throughout this paper.

Another approach is to use the full NS equations to derive the force taking into account all the terms. With this approach an issue is encountered regarding the number of unknowns. In conventional pressure driven flows the only unknown is the pressure gradient which can be derived using Eq.6 since the velocity field is already known. In the case of the plasma actuator though, the body force term appears as one extra unknown. To be able to bypass this problem two major assumptions must be made: 1) the body-force remains steady or quasisteady in time and 2) the pressure gradient prior to the actuation is zero. With these assumptions Eq.6 is differentiated in time:

$$\frac{\partial^2 \vec{U}}{\partial t^2} + \frac{\partial (\vec{U} \cdot \nabla \vec{U})}{\partial t} - \nu \, \frac{\partial (\nabla^2 \vec{U})}{\partial t} = -\frac{\partial (\nabla p)}{\partial t} \tag{8}$$

Based on the first assumption the time derivative of the body force becomes zero. Integrating Eq.8 back in time the pressure gradient can be calculated. Based on an initial condition of zero pressure gradient, the integration constant A is reduced to zero.

$$\int_0^t (\frac{\partial^2 \vec{U}}{\partial t^2} + \frac{\partial (\vec{U} \cdot \nabla \vec{U})}{\partial t} - \nu \, \frac{\partial (\nabla^2 \vec{U})}{\partial t}) dt = -(\nabla p) + A \tag{9}$$

Eq.9 is plugged back into Eq.6 and leaves the body force term as the only unknown. Since the time gradient of the NS is used, this method will be referenced as the 'gradient method' throughout this paper. In contrast to the previous techniques the reduced and gradient methods have the considerable advantage of resolving not only the magnitude of the body force but also its spatial distribution as well as its direction. The results from such analysis can be valuable for validation of numerical models of plasma actuators as well as an input into flow solvers investigating flow control applications using these actuators.

III. Experimental Setup

A. The actuator

For this study Dielectric Barrier Discharge (DBD) actuators are used. The actuators consist of thin rectangular copper electrodes made out of self-adhesive copper tape separated by a dielectric layer (Fig.1). The thickness of the electrodes is 60 μm while the width varies between 5 mm and 25 mm depending on the test case. Their effective spanwise length (along which plasma is generated) is 300 mm for the load cell measurements and 200 mm for the PIV measurements. The electrodes are separated by several Kapton tape layers. The thickness of each layer is 2 mil (50.8 μm). For the entire study, no more than three layers were used keeping the total thickness of the dielectric below ca. 150 microns. The upper electrode is connected to the HV output cable of a TREK 20/20C HV amplifier (20 kV_{pp}, 20 mA, 1000 W) while the lower electrode is grounded.

The actuator operation is controlled remotely via a computer workstation were the driving signal is created by software and is sent to the amplifier via a Digital/Analog (D/A) converter. The amplifier provides direct readings of the output voltage and current through internal measurement probes. While the internal voltage probe gives sufficiently accurate readings the internal current probe has been found to be too slow

to resolve high frequency current fluctuations. This is typically the case with discharge currents occurring during plasma actuators operation. To resolve this, a resistance is placed between the lower electrode and the grounding cable and voltage is measured across it indicating the influx of current.

To reduce the effect of any external disturbances on the measurements, the tests are ran in still air. To ensure this, a test box is constructed from clear Plexiglas. The box is used in all cases involving both load cell and PIV measurements.

For the direct thrust measurements several actuators are tested with variations in parameters such as length of electrodes, horizontal gap, voltage and carrier frequency. Due to the conceptual stage of the PIV investigation, only one actuator is tested with this method. This incorporates upper and lower electrodes of 10 mm length, with zero horizontal gap and 100 μm of dielectric thickness. For this actuator voltages of 8 to 16 kV_{pp} and carrier frequencies of 1 to 4 kHz are tested. An overview of the actuator parameters for all measurements is shown in Tab.1.

Table 1. Test cases for thrust and body force investigation

Direct thrust measurements		
parameter	**value**	**base value**
upper electrode length (l_u)	5, 10, 15 mm	10 mm
lower electrode length (l_l)	5, 10, 15 mm	10 mm
dielectric thickness (t_d)	50, 100, 150 μm	100 μm
horizontal gap (g)	-2.5, -1, 0, 1.5, 2.5 mm	0 mm
applied voltage (V_{app})	-	*
frequency (F)	-	*
*for geometrical test cases		
all possible combinations of:		
applied voltage (V_{app})	6, 8, 10, 12, 14 kV_{pp}	
	×	
frequency (F)	0.5, 1, 1.5, 2, 2.5, 3 kHz	
PIV measurements		
parameter	**value**	**base value**
upper electrode length (l_u)	10 mm	-
lower electrode length (l_l)	10 mm	-
dielectric thickness (t_d)	100 μm	-
horizontal gap (g)	0 mm	-
applied voltage (V_{app})	8 to 16 kV_{pp} (steps of 2 kV)	10 kV_{pp}
frequency (F)	1 to 4 kHz (steps of 1 kHz)	2 kHz

B. Load cell

For the direct thrust measurements, an electronic strain-gage load cell is used. A light Plexiglas plate of 5 mm thickness, which carries the electrodes and dielectric, is directly mounted on the load cell. The connection of the electrodes to the HV and ground connectors is done via thin copper wires to minimize disturbances coming from the cables. Each test case is measured three times in order to minimize the influence from any load cell relaxation. The measurement is done for ten seconds before actuation and thirty seconds after in order to ensure steady conditions. The thrust is then calculated by comparing the time averaged readings of the load cell from the two time periods.

C. PIV setup

High speed PIV has been applied to characterize the flow field in the vicinity of the plasma actuator. This technique provides the required spatial and temporal resolution in order to characterize the transient behavior of the thin wall jet formed by the plasma actuator. A two component PIV configuration has been chosen since the span length of the actuator allows the assumption of two dimensional flow for the mid-span area.

The space in the Plexiglas box is seeded with approximately 1 micron olive oil droplets generated by a TSI atomizer. The particles at the mid span of the actuator are illuminated by a light sheet of $2mm$ thickness generated by a Quantronix Darwin-Duo laser system with an average output of 80 W at 3 kHz. A Photron Fastcam SA1 high speed CCD camera of 1024×1024 pixels (full sensor size) is used to capture the field-of-view (FOV). Image acquisitions have been conducted at 10 KHz rate in single-frame mode. A Nikkor 105 mm macro lens is used with extension tubes in order to achieve 0.8 magnification and a FOV of 15×6 mm imaged by cropping the image at 10KHz. The images are analyzed using Davis 7.4 (Lavision GmbH) with final integration window size of 12×12 pixels and overlap factor of 75%. The interrogation windows have been weighted using 4:1 aspect ratio in order to obtain higher spatial resolution in the wall normal direction.

IV. Results

A. Load cell thrust measurements

Due to the flexibility the load cell approach offers, a large number of test cases can be tested within a relatively short time span. A parametric study has therefore been conducted in order to assemble a benchmark database for future comparison with more time and resource demanding techniques such as the proposed PIV method.

Thrust measurements are taken for four geometrical parameters of the plasma actuator, namely upper (l_u) and lower (l_l) electrode lengths, dielectric thickness (t_d) and horizontal gap (g) (Fig.3). For each test case a sub-matrix of applied voltages between 6 kV_{pp} and 14 kV_{pp} and frequencies between 0.5 kHz and 3 kHz is constructed and all combinations are tested. The overview of the parameters tested is shown in Tab.1. The parametric study is done in a 'ceteris paribus' approach where for each test case the investigated parameter is the only variable while all other parameters are kept constant. For every test case the first column in Tab.1 indicates the investigated parameter, the second column gives the tested range of values and the third column indicates the constant base value of the parameter for all other cases.

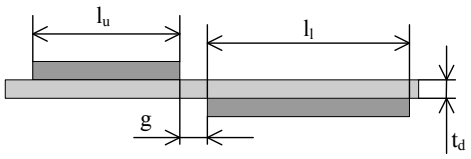

Figure 3. The geometrical properties of the plasma actuator

Thrust for the lower electrode length variation is shown in figure 4(a). The value appears to be independent to any change in length. Measurements for the variation of the horizontal electrode gap are shown in figure 4(b). Positive gaps seem to have a reducing effect on the intensity of the electric field and all induced quantities including body force. For negative gaps no significant dependence of the force exists although the traveling current and thus the power consumption increase considerably. For the case of 14 kV_{pp} no negative gap measurements are taken due to the destruction of the dielectric by the increased discharge current.

To this point it is clear that there is a thrust dependence on applied voltage. Geometrical parameters are also influencing thrust magnitude albeit to a lesser degree. In order to gain more insight into the relation of thrust and voltage, a fine grid of frequencies and voltages is devised and a new actuator is tested. The tested actuator has an upper electrode length (l_u) of 5 mm, lower electrode length (l_l) of 10 mm and zero horizontal electrode gap (g). Dielectric thickness (t_d) is 0.1 mm. As with the previous investigations, the spanwise length of the actuator (l_a) is 300 mm. The frequency range lies between 0.5 and 4 kHz with a step size of 0.25 kHz while the applied voltage values span from 5 to 15 kV_{pp} in steps of 0.5 kV. The upper right area of the grid, which consists of high voltages and high frequencies, is not tested due to the HV amplifier slew-rate limitations. Simultaneous to the thrust measurements, discharge current is also measured in order to calculate the power consumption.

From the results of the fine grid investigation, several observations can be made on the behavior of thrust and power consumption. Thrust and in extension body force appear to be connected with voltage through a power law as it is already observed from the geometrical properties investigation, while the relation with frequency is linear. This agrees with observations made by previous investigations.[16,18] Additionally,

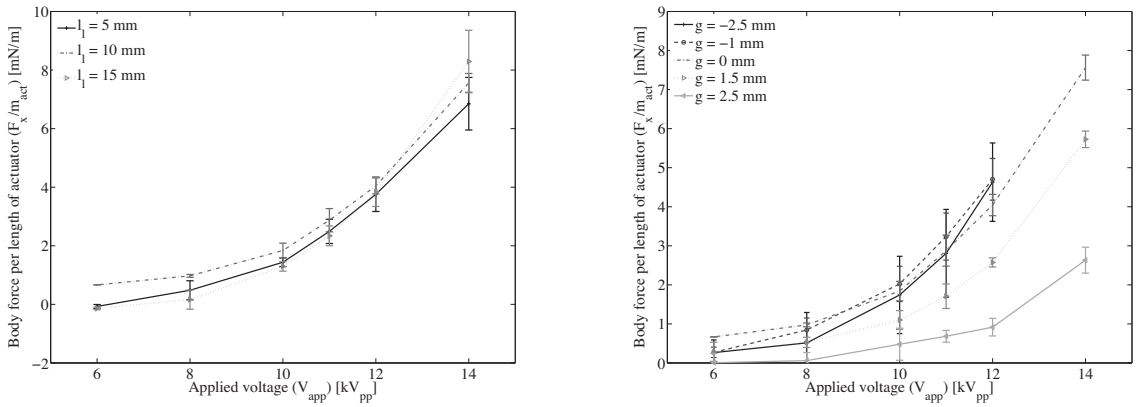

Figure 4. Thrust measurements for lower electrode length (l_l) variation (a) and horizontal electrode gap (g) variation (b). Frequency (F) is 2 kHz

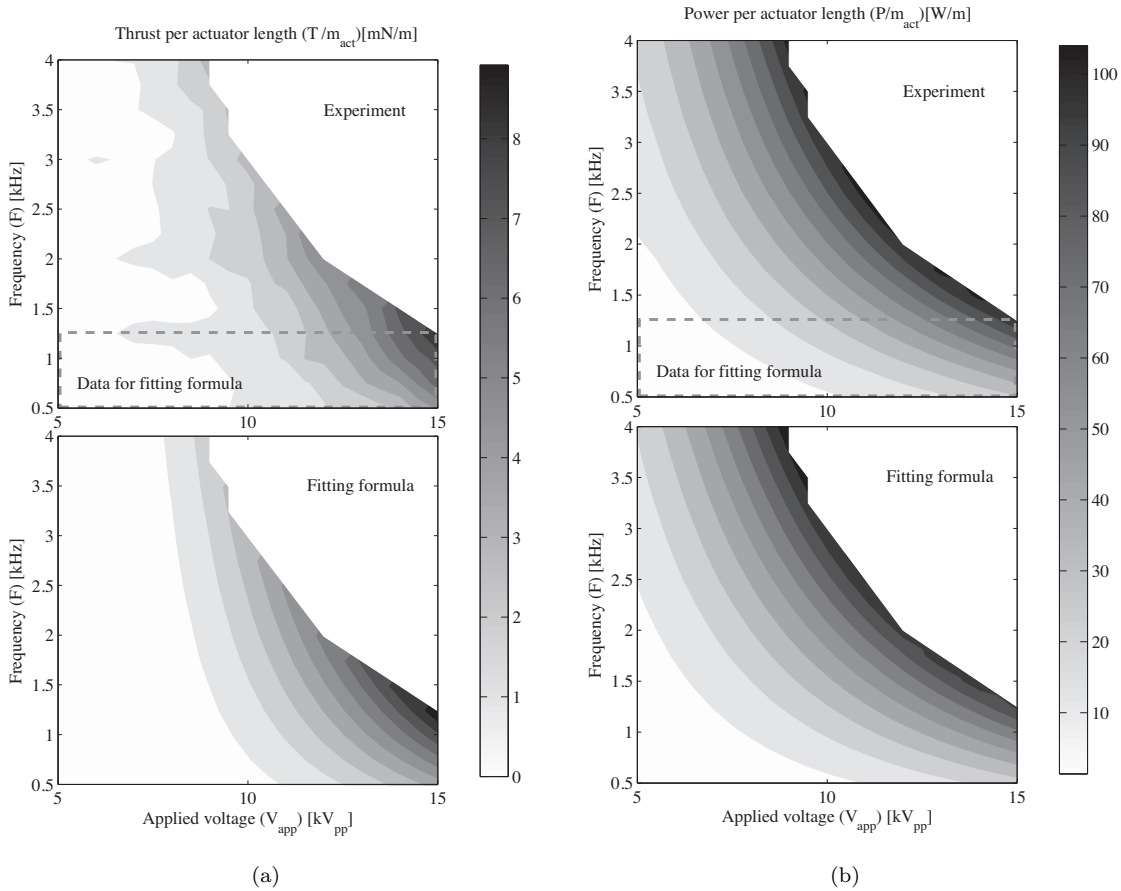

Figure 5. Experimental and modeled thrust (a) and power (b) for voltage and frequency variation.

the existence of a threshold voltage value of approximately 5 kV_{pp} is confirmed. Below this threshold, no detectable body force exists. For the power consumption, a similar power law exists in relation to the applied voltage. Diverging from the body force case, a weak power law applies also in relation to the frequency. This weak power law dependence has not been reported by any previous investigations. Based on the observed behavior, two fitting formulas can be derived connecting voltage (V_{app}) and frequency (F) with thrust (T) and power consumption (P) respectively. F_b and P are considered to be normalized with the spanwise length of the actuator (l_a). It is repeated here that the value of thrust includes the shear force on the flat surface.

$$T = \frac{a \cdot F \cdot (V_{app} - V_0)^b}{l_a} \tag{10}$$

$$P = \frac{c \cdot F^d \cdot (V_{app})^e}{l_a} \tag{11}$$

Coefficients a and c correspond to the influence of discharge dynamics and actuator geometry while coefficients b and e define the power law on the voltage. The value of d defines the weak power law that connects frequency and power. The factor V_0 accounts for the non-zero voltage threshold below which no significant body force is observed.

For deriving the coefficients of Eq.10 and Eq.11, data from the fine grid investigation is fitted only for a range of frequencies from 0.5 to 1.25 kHz were high voltage values can be reached by the amplifier and thus the values of the body force are relatively large. The coefficients for the current actuator are shown in Tab.2. Comparison of experimental and modeled thrust and power values is shown in Fig.5(a) and Fig.5(b) respectively. Despite the fact that the coefficients of the formulas are derived from fitting only part of the measurement data, the formulas describe the mechanics of the actuator well across the entire grid. Average error is 3.8% for body force and 2% for power estimation. Maximum errors are 14% and 5.8% respectively. All errors are referenced in respect to the maximum experimental values of force and power. It is important to note that the formulas described by Eq.10 and Eq.11 are only valid for the tested range of frequencies and voltages. Regarding the power law connecting voltage with thrust and power, the values of the exponent (coefficients b and e) lie between similar reported values,[18–20] although these researchers used thicker dielectrics.

Table 2. Fitting coefficients for the fine grid investigation

coefficient	value	
a	$1.29 \cdot 10^{-2}$	$mN/kHz{\cdot}kV^b$
b	2.798	
c	$4.29 \cdot 10^{-2}$	$mN/kHz^d{\cdot}kV^e$
d	1.35	
e	2.738	
V_0	5 kV	

B. PIV measurements: estimation of thrust

For the estimation of thrust using the momentum balance technique the dataset from the high speed PIV measurement is used. After the initial acceleration stage the induced flow field is fully developed into a laminar wall jet. The momentum balance equations are used in time-steady form thus the flow field must have reached the steady state before data can be used. Steady state is reached in approximately 30 ms after actuation. In this respect is safe to average for approximately 400 frames spanning from 43 ms after the actuation to 83 ms. Apart from the processing of the raw PIV data and time averaging no other filtering or smoothing has been applied.

Table 3. Section contribution in thrust (mN/m_{act}) for case of 12 kV_{pp}, 2 kHz

section	x-thrust	y-thrust
bc	-0.131	0.0015
cd	0.0160	-0.1344
da	3.9828	-0.0235
$total$	3.8673	-0.1564

The time averaged flow field with the selected control volume is shown in Fig.6. It is obvious that the majority of momentum increase occurs in the x direction while a weak suction effect is observed upstream the inner edge of the electrodes. The suction effect is an indication of a pressure gradient which is potentially strong at the vicinity of the actuator. As mentioned in the methodology description any existing pressure gradient cannot be readily resolved using the time

averaged velocity data. It is therefore necessary to chose a control volume such that the effects of pressure are minimized.

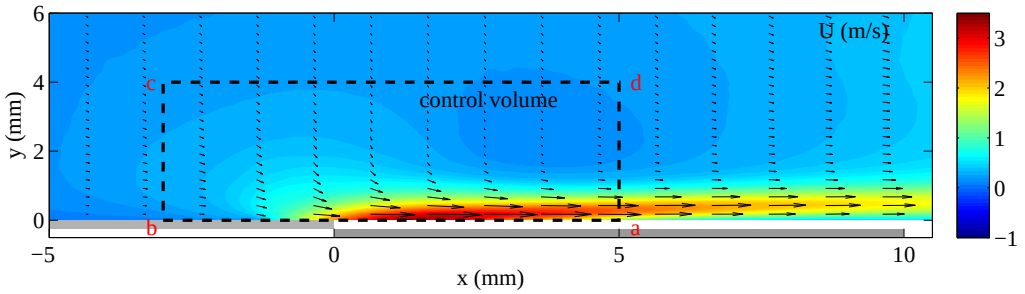

Figure 6. Time averaged total velocity field and control volume for momentum balance (12kV_{pp}, 2 kHz)

In applying the momentum balance equation in direction x and y reveals the significance of each of the boundaries of the control volume. As is shown in Tab.3 and also apparent from the velocity field, the maximum contribution to thrust comes from the outflowing horizontal velocity from section *ad*. This implies that the very simple approach of calculating thrust from only one cross section of the jet would still deliver satisfying results. Nevertheless since field data are available the method used herein takes into account all sections of the control volume.

In comparing the calculated thrust from the PIV data with the direct thrust measurement using the load cell, small discrepancies exist. These could be attributed to the three dimensional effects near the edges of the actuator in the load cell case. Although these exist in the PIV case as well, they are not transfered in the results since thrust is calculated from velocity data at the mid-span of the actuator. Nevertheless the thrust value from the momentum balance analysis falls well into the error margin of the load cell measurements.

C. PIV measurements: estimation of body force

The technique of resolving the body force from velocity data is applied on the dataset from the PIV measurements. As previously mentioned this can be done via two approaches, namely using only the initial steady acceleration of the flow (reduced method) or using the full NS equations (gradient method). The flow field evolution is presented in Fig.7.

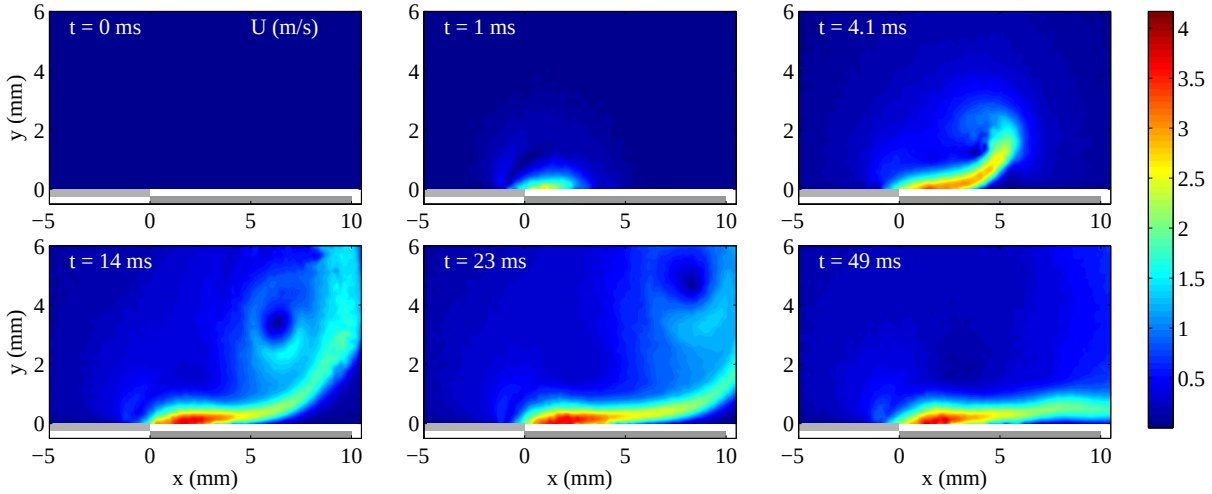

Figure 7. The temporal evolution of the total velocity field (U) for the actuation case of 12 kV_{pp}, 2 kHz. No processing on the data.

The flow reacts very fast to the actuation with initial velocity components already starting to appear approximately 0.5 ms after the start of the actuation. The flow accelerates in a region starting from the

end of the upper electrode and extending over half the covered electrode. A strong starting vortex is also evident which develops and convects out of the FOV in less than 40 ms after the start of the actuation.

At this point, some specific features of the induced flow field should be discussed due to their effect on the results of the proposed technique. In a previous study[21] high frequency velocity fluctuations are registered in the vicinity of the actuator. These fluctuations are a product of the carrier frequency at which the actuator is operating. More specifically it appears that the two half-cycles of the sinusoidal HV do not contribute equally to the momentum transfer from the ionized gas to the neutral air. These fluctuations appear in the current PIV measurements corresponding to the carrier frequency for each case. The analysis of this behavior does not fall in the scope of this paper and will be described in subsequent reports.

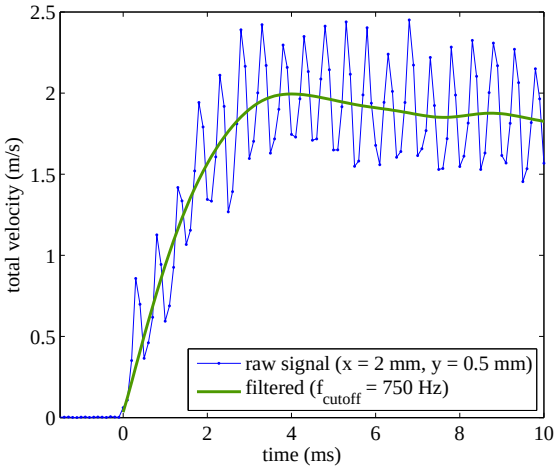

Figure 8. Time evolution of velocity

The proposed method relies on the resolution of the accelerating flow and interpretation of that to a body force. In this process the first and second time derivatives of velocity are required. Due to the high frequency fluctuations, these terms cannot be resolved without large artifacts. Based on the large difference between the time scale governing the acceleration of the flow from quiescent conditions to fully developed jet and the time scale of these fluctuations one further assumption must be made. This states that although the flow, and in extent the body force, fluctuate in time the later can be considered as quasi steady. This is further encouraged by the fact that the rise time of the flow (accelerating part) is considerably larger than the fluctuation period. In this fashion the PIV series of flow field snapshots is filtered with a 4th order low-pass Chebychev filter (Fig.8). The cutoff frequency is chosen based on the carrier frequency of the HV signal corresponding to the test case under investigation.

As already mentioned in the methodology section, the reduced method involves the utilization of the very first moments after actuation when all other terms apart from acceleration can be neglected. The acceleration, convective, viscous and pressure gradient components of the NS are shown in Fig.9 as a function of time after actuation. As expected the acceleration term dominates the very first moments of actuation with a high and almost constant value. Convection and pressure gradient eventually dominate the event while viscous effects have a constant and moderate influence. It should be mentioned here that the pressure gradient term is calculated using the gradient method as discussed in section C. Although no real metric is available to determine the exact time span of the initial 'pure' acceleration stage, a semi-arbitrary span of 1 ms seems to provide reasonable results.

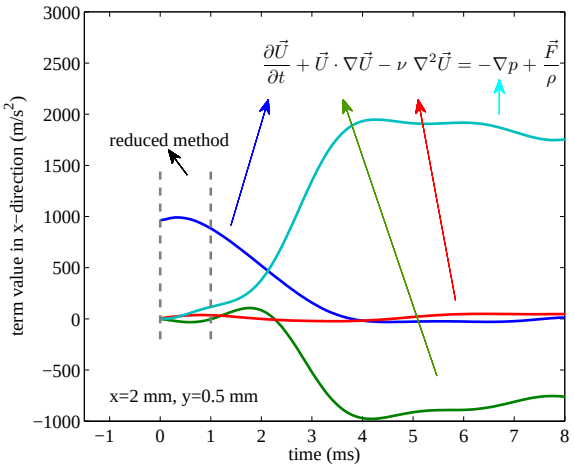

Figure 9. Evolution over time of the NS terms governing the development of the flow in x direction ($12kV_{pp}$, $2kHz$)

The spatial distribution of the body force as calculated by the reduced method is shown in Fig.10 for the case of $12kV_{pp}$ applied voltage and $2kHz$ carrier frequency. The frames used for this case cover the first 0.8 ms after actuation and the force field is simply averaged over this span. The bulk of the force appears to be just downstream the inner electrode edge while the horizontal extent spans almost a quarter of the covered electrode. In the wall normal direction the force field extends no more than 1 mm which

confirms the very thin wall jet reported by this and numerous other investigations. The vertical force seems to be very weak compared to the horizontal component. For this case the cutoff frequency of the Chebychev filter is 750 Hz.

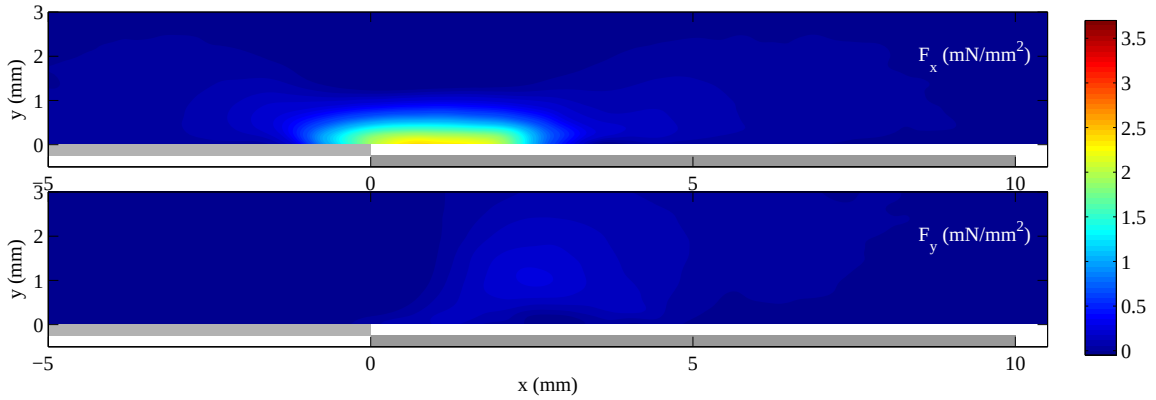

Figure 10. Spatial distribution of the body force using the reduced method ($12kV_{pp}$, $2kHz$).

For the same case the spatial distribution of the body force using the gradient method is shown in Fig.11. For this case the first 20 ms after actuation are used and the final force field is averaged over this span. The general shape of the field is identical to the results from the reduced method.

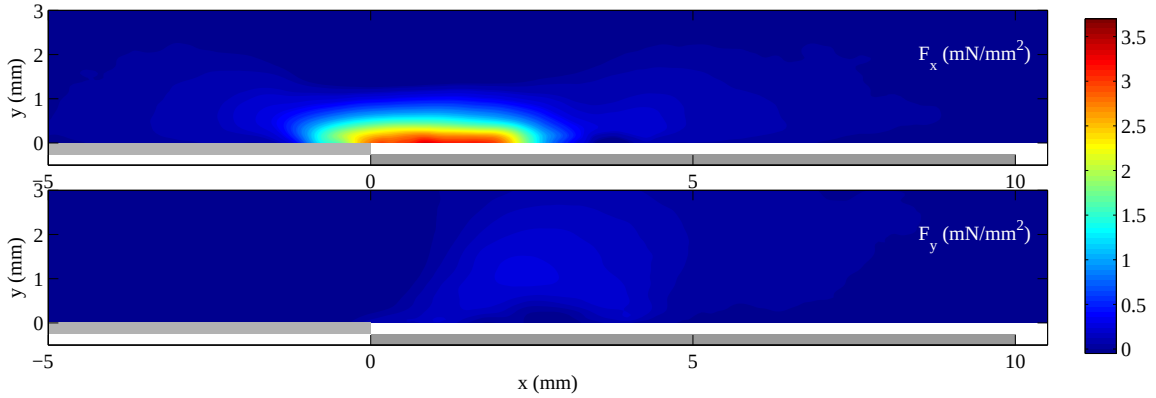

Figure 11. Spatial distribution of the body force using the gradient method ($12kV_{pp}$, $2kHz$).

A small discrepancy exists in the intensity of the force field which can be attributed to modeling errors inherent in the term elimination of the reduced method. Nevertheless the agreement between the two techniques seems to be sufficient. Additionally and in contrast to the reduced method, the gradient method is not limited in the time span of application. Applying this method for the first 20 ms after actuation gives an almost constant in time body force distribution. Several snapshots of the instantaneous total force field are shown in Fig.13 . The temporal stability of the force distribution is one extra indication of the validity of the method as this was an important assumption made during the formulation of the technique.

A comparison on the thrust values attained by all the investigated techniques is given in Tab.4 for the test case of $12kV_{pp}$ and 2 kHz. For the PIV methods thrust is calculated simply by integrating the force distribution over the 2D space domain. As already mentioned

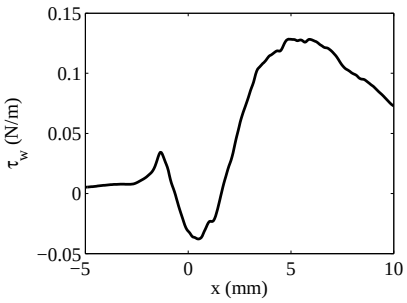

Figure 12. Shear stress at the wall along x direction

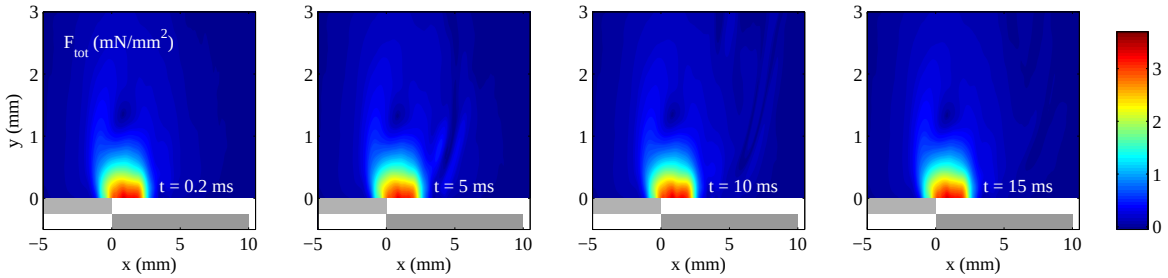

Figure 13. Instantaneous total force field obtained using the gradient method ($12kV_{pp}$, $2kHz$).

the thrust values from the load cell measurement and momentum balance analysis contain the contribution of the actuator as well as the shear stress between the jet and the surface.

Comparing the thrust value from the momentum balance to the two PIV methods, some interesting comments can be made. The horizontal component of thrust in both PIV methods is larger than the momentum balance value. Yet the vertical component is in excellent agreement especially in the case of the gradient method. This implies that the difference in x-direction could be attributed in shear stresses between the flow and the flat surface. These simply do not exist in y-direction and act always in the direction opposite to the flow. A rough calculation based on the velocity gradient of the field at the wall gives the shear stress along the stream wise direction (Fig.12). Although the FOV is not sufficient to resolve further than 10 mm downstream the actuator, an integration over the available span gives a shear stress of 0.9 mN. This, added to the momentum balance thrust, brings the result even closer to the PIV method's values.

V. Conclusions

An experimental study on the thrust and body force production by Dielectric Barrier Discharge actuators has been conducted. A simple and robust technique of direct thrust measurement using a highly sensitive load cell was firstly used. With this technique a parametric study has been conducted on thrust with varying parameters such as electrode lengths, voltage and frequency. A power law has been verified to describe the evolution of thrust with voltage while the relationship with frequency has been found to be linear.

A second technique based on momentum balance of the developed flow field has also been applied. The flow field has been attained using a 2D high speed PIV system. The time averaged flow field has been analyzed using a control volume approach and results show thrust values in the range of the respective load cell test case. Small discrepancies can be attributed to the three-dimensionality of the induced flow field near the edges of the actuator. This is registered during the load cell measurement but not during the PIV run. It should be noted that PIV data is not a necessity for this method. It is shown that only with the outflow cross section velocities known, reliable results can be achieved. The time and effort resources for this technique could be kept to a minimum if velocities from one or more cross sections are measured using pilot tubes or hot wires.

Table 4. Thrust calculation from the tested techniques (mN/m_{act}) for case of 12 kV_{pp}, 2 kHz

technique	x-thrust	y-thrust
load cell	4.012	-
momentum balance	3.860	-0.156
reduced PIV	4.202	-0.084
gradient PIV	5.679	-0.149

To alleviate some of the drawbacks of the previous two techniques and mainly to acquire the spatial distribution of the force field a novel technique is proposed, developed and tested. This involves the time resolved measurement of the evolving flow field with a 2D high speed PIV system. Through decomposition of the velocity field in the NS terms, the body force can be calculated. This can be done either using a reduced form of the equations or using the full equations. Initial results demonstrate the feasibility of the method while the calculated values show excellent agreement with the previously established thrust measurements.

Future work involves the application of the developed PIV technique for a full parametric study on the variation of body force with several operational parameters of the actuator. This can subsequently be used as a database for flow solvers incorporating plasma actuator techniques.

Acknowledgments

This work is done in the framework of the CleanEra project at the TU Delft (www.cleanera.tudelft.nl). The authors would like to thank Prof. Fulvio Scarano for his valuable contribution and to acknowledge Leo Molenwijk and Stefan Bernardy for their technical assistance.

References

[1]Post, M. L. and Corke, T. C., "Separation control on high angle of attack airfoil using plasma actuators," *AIAA Journal*, Vol. 42, No. 11, 2004, pp. 2177–2184.

[2]Jukes, T. N., Choi, K. ., Johnson, G. A., and Scott, S. J., "Turbulent drag reduction by surface plasma through spanwise flow oscillation," *3rd AIAA Flow Control Conference*, Vol. 3, 2006, pp. 1687–1700.

[3]Jacob, J. D., Rivir, R., Carter, C., and Estevadeordal, J., "Boundary layer flow control using AC discharge plasma actuators," *2nd AIAA Flow Control Conference*, 2004.

[4]Huang, J., Corke, T. C., and Thomas, F. O., "Plasma Actuators for Separation Control of Low-Pressure Turbine Blades," *AIAA Journal*, Vol. 44, 2006, pp. 51–57.

[5]Seraudie, A., Aubert, E., Naude, N., and Cambronne, J. P., "Effect of plasma actuators on a flat plate laminar boundary layer in subsonic conditions," *3rd AIAA Flow Control Conference*, Vol. 2, 2006, pp. 1065–1073.

[6]Grundmann, S. and Tropea, C., "Active cancellation of artificially introduced Tollmien-Schlichting waves using plasma actuators," *Experiments in Fluids*, Vol. 44, No. 5, 2008, pp. 795–806.

[7]Moreau, E., "Airflow control by non-thermal plasma actuators," *Journal of Physics D: Applied Physics*, Vol. 40, No. 3, 2007, pp. 605–636.

[8]Corke, T. C., Post, M. L., and Orlov, D. M., "SDBD plasma enhanced aerodynamics: concepts, optimization and applications," *Progress in Aerospace Sciences*, Vol. 43, No. 7-8, 2007, pp. 193–217.

[9]Jayaraman, B., Cho, Y. ., and Shyy, W., "Modeling of dielectric barrier discharge plasma actuator," *38th AIAA Plasmadynamics and Lasers Conference*, Vol. 2, 2007, pp. 1019–1038.

[10]Lagmich, Y., Callegari, T., Pitchford, L. C., and Boeuf, J. P., "Model description of surface dielectric barrier discharges for flow control," *Journal of Physics D: Applied Physics*, Vol. 41, No. 9, 2008.

[11]Jayaraman, B. and Shyy, W., "Modeling of dielectric barrier discharge-induced fluid dynamics and heat transfer," *Progress in Aerospace Sciences*, Vol. 44, No. 3, 2008, pp. 139–191.

[12]Singh, K. P., Roy, S., and Gaitonde, D. V., "Modeling of dielectric barrier discharge plasma actuator with atmospheric air chemistry," Vol. 2, 2006, pp. 576–586.

[13]Orlov, D. M., Apker, T., He, C., Othman, H., and Corke, T. C., "Modeling and experiment of leading edge separation control using SDBD plasma actuators," Vol. 15, 2007, pp. 10651–10668.

[14]Likhanskii, A. V., Shneider, M. N., Opaits, D. F., Miles, R. B., and Macheret, S. O., "Numerical modeling of DBD plasma actuators and the induced air flow," *38th AIAA Plasmadynamics and Lasers Conference*, Vol. 2, 2007, pp. 1060–1072.

[15]He, C., Corke, T. C., and Patel, M. P., "Numerical and experimental analysis of plasma flow control over a hump model," Tech. rep., 2007.

[16]Abe, T., Takizawa, Y., Sato, S., and Kimura, N., "Experimental study for momentum transfer in a dielectric barrier discharge plasma actuator," *AIAA Journal*, Vol. 46, No. 9, 2008, pp. 2248–2256.

[17]Enloe, C. L., McHarg, M. G., and McLaughlin, T. E., "Time-correlated force production measurements of the dielectric barrier discharge plasma aerodynamic actuator," *Journal of Applied Physics*, Vol. 103, No. 7, 2008, Cited By (since 1996): 1.

[18]Enloe, C. L., McLaughlin, T. E., VanDyken, R. D., Kachner, K. D., Jumper, E. J., and Corke, T. C., "Mechanisms and Responses of a Single Dielectric Barrier Plasma Actuator: Plasma Morphology," *AIAA Journal*, Vol. 42, No. 3, 2004, pp. 589–594.

[19]Dong, B., Bauchire, J. M., Pouvesle, J. M., Magnier, P., and Hong, D., "Experimental study of a DBD surface discharge for the active control of subsonic airflow," *Journal of Physics D: Applied Physics*, Vol. 41, No. 15, 2008.

[20]Forte, M., Jolibois, J., Pons, J., Moreau, E., Touchard, G., and Cazalens, M., "Optimization of a dielectric barrier discharge actuator by stationary and non-stationary measurements of the induced flow velocity: Application to airflow control," *Experiments in Fluids*, Vol. 43, No. 6, 2007, pp. 917–928.

[21]Benard, N. and Moreau, E., "Capabilities of the dielectric barrier discharge plasma actuator for multi-frequency excitations," *Journal of Physics D: Applied Physics*, Vol. 43, No. 14, 2010.